Specific electrostatic interactions between charged amino acid residues regulate binding of von Willebrand factor to blood platelets

Received for publication, May 17, 2017, and in revised form, August 25, 2017 Published, Papers in Press, September 18, 2017, DOI 10.1074/jbc.M117.797456

Gianluca Interlandi[‡1,2], Olga Yakovenko[‡1], An-Yue Tu[‡], Jeff Harris[§], Jennie Le[§], Junmei Chen[§], José A. López[§¶], and Wendy E. Thomas[‡3]

From the [‡]Department of Bioengineering, University of Washington, Seattle, Washington 98195, the [§]Bloodworks Research Institute, Seattle, Washington 98102, and the [¶]Departments of Medicine, Biochemistry, and Mechanical Engineering, University of Washington, Seattle, Washington 98195

Edited by Norma Allewell

The plasma protein von Willebrand factor (VWF) is essential for hemostasis initiation at sites of vascular injury. The platelet-binding A1 domain of VWF is connected to the VWF N-terminally located D′D3 domain through a relatively unstructured amino acid sequence, called here the N-terminal linker. This region has previously been shown to inhibit the binding of VWF to the platelet surface receptor glycoprotein Ibα (GpIbα). However, the molecular mechanism underlying the inhibitory function of the N-terminal linker has not been elucidated. Here, we show that an aspartate at position 1261 is the most critical residue of the N-terminal linker for inhibiting binding of the VWF A1 domain to GpIbα on platelets in blood flow. Through a combination of molecular dynamics simulations, mutagenesis, and A1–GpIbα binding experiments, we identified a network of salt bridges between Asp[1261] and the rest of A1 that lock the N-terminal linker in place such that it reduces binding to GpIbα. Mutations aimed at disrupting any of these salt bridges activated binding unless the mutated residue also formed a salt bridge with GpIbα, in which case the mutations inhibited the binding. These results show that interactions between charged amino acid residues are important both to directly stabilize the A1–GpIbα complex and to indirectly destabilize the complex through the N-terminal linker.

The protein von Willebrand factor (VWF)[4] is essential to initiate hemostasis at sites of vascular injury with high blood flow (1). The A1 domain of VWF binds to glycoprotein Ibα (GpIbα) on the surface of blood platelets (2), whereas the A3 domain binds to collagen in the exposed endothelium. This provides an initial tethering mechanism of platelets to the site of vascular injury. Under normal conditions, circulating VWF does not significantly bind to platelets (3). However, VWF becomes activated either under high shear stress (4) or when it is bound to collagen at the site of exposed endothelium (2). These characteristics motivated our investigation into the structural properties that modulate the binding of the A1 domain to GpIbα.

The A1 domain of VWF presents a globular fold (Fig. 1*a*) with a relatively long N-terminal sequence that links it to the neighboring D′D3 domain and a shorter C-terminal sequence that connects to the A2 domain (Fig. 1*b*). An important feature of the A1 domain is the presence of a disulfide bond between Cys[1272] and Cys[1458] (5) (Fig. 1*a*). We refer to the region within the loop defined by this disulfide bond (Fig. 1*b*) as the "core" A1 domain and the 34 amino acids connecting Cys[1237] at the end of the D′D3 domain to Cys[1272] at the start of the core A1 domain as the N-terminal linker (Fig. 1*b*). There is compelling experimental evidence that the N-terminal linker plays an inhibitory function in the binding between A1 and GpIbα. One of the first studies that provided such evidence showed that a construct with no N-terminal linker bound to GpIbα much more strongly in static conditions than both a construct containing half of the N-terminal linker and another construct that contained the entire linker and part of the D′D3 domain (6). In another study, binding of platelets to recombinant A1 domain immobilized on a surface was tested in dynamic flow conditions (7). Variants of A1 that contained the entire N-terminal linker and part of the D′D3 domain (Fig. 1*b*) mediated rolling adhesion in a similar fashion as full-length VWF. In contrast, variants of A1 without the N-terminal linker (starting at position 1271 right next to the disulfide bond) mediated strong stationary adhesion (7).

Unfortunately, it is difficult to infer the molecular mechanism behind the inhibitory function of the N-terminal linker because currently no crystallographic structures of the A1 domain have been reported that include the entire N-terminal sequence. Of the 34 amino acids in the N-terminal linker, a maximum of 13 have been included in the constructs used in the crystallographic studies, and the electron density and coor-

This work was supported by a National Institutes of Health Career Development Award K25HL118137 (to G. I.) and National Institutes of Health Grants R01HL106074 (to W. E. T.) and R01HL117639, R01HL112633, and R21HL129526 (to J. A. L.). The authors declare that they have no conflicts of interest with the contents of this article. The content is solely the responsibility of the authors and does not necessarily represent the official views of the National Institutes of Health.
This article contains supplemental Fig. S1.

[1] Both authors contributed equally to this work.

[2] To whom correspondence may be addressed: Dept. of Bioengineering, University of Washington, Box 355061, 3720 15th Ave. NE, Seattle, WA 98195-5061. Tel.: 206-685-4435, Fax: 206-685-3300, E-mail: gianluca@u.washington.edu.
[3] To whom correspondence may be addressed. Tel.: 206-616-3947; Fax: 206-685-3300, E-mail: wendyt@uw.edu.

[4] The abbreviations used are: VWF, von Willebrand factor; GpIbα, glycoprotein Ibα; MD, molecular dynamics; flVWF, full-length VWF; RMSD, root mean square deviation; RMSF, root mean square fluctuations; PDB, Protein Data Bank.

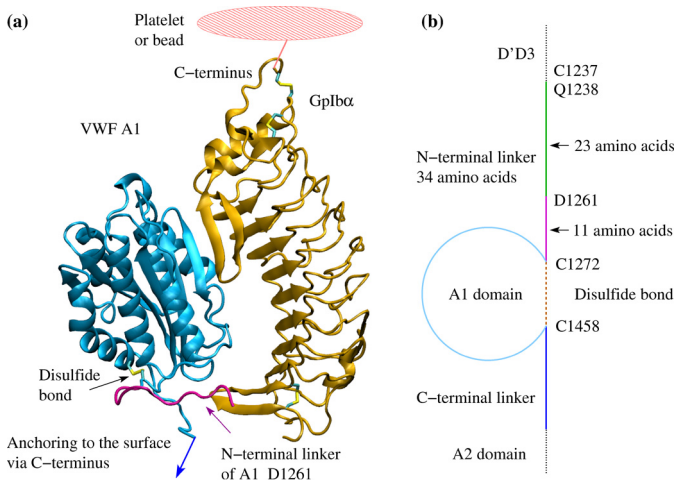

Figure 1. Complex between VWF A1 and GpIbα and amino acid sequence of the A1 domain. *a*, three-dimensional structure of the complex between A1 and GpIbα used in this manuscript. The structure was derived from the complex co-crystallized with botrocetin (PDB code 1U0N) (8), because this is the only structure of the complex where 11 amino acids of the A1 N-terminal linker were resolved (other structures had less). The backbone of the A1 N-terminal linker resolved in the X-ray structure (containing 11 amino acids) is highlighted in *magenta*. The disulfide bond between Cys^{1272} and Cys^{1458} is shown. Also indicated are the anchoring of the C terminus of GpIbα to blood platelets or beads and the attachment of the C terminus of the A1 domain to either a neighboring domain or directly to the surface. *b*, schematic representation of the A1 domain core with the disulfide bond and N- and C-terminal linkers. The elements in this figure are not to scale.

dinates were resolved for at most 11 of these amino acids. The structures with these 11 residues resolved were the isolated A1 (5) and the complex of A1, GpIbα, and botrocetin (8) (shown in Fig. 1, although botrocetin is not displayed). These 11 amino acids are located in proximity of the rest of the A1 domain in both of these structures, but they are not seen to interact with GpIbα in the structure of the complex (Fig. 1). This leaves the question open of how these 11 and the remaining 23 amino acids regulate binding of A1 to GpIbα.

The role of the N-terminal linker in regulating the A1 domain became even more intriguing after the discovery through single molecule force spectroscopy experiments that the lifetime of the bond between A1 with the entire N-terminal linker and GpIbα increases with force (9), which is the characteristic of a catch bond. Catch bonds have also been observed for the bacterial adhesin FimH (10), myosin (11), selectins (12), and integrins (13) bound to their respective targets. A later single molecule force spectroscopy study showed that shortening the N-terminal linker to the 11 amino acids closest to the disulfide bond (*i.e.* starting at position 1261 similarly to the sequence seen in X-ray structures; *e.g.* Fig. 1) eliminates catch-bond behavior and converts the bond between A1 and GpIbα to a slip bond (14), for which lifetime decreases with increasing tensile force. However, two studies drew opposite conclusions about why the entire N-terminal linker was required for catch bond behavior and shear-enhanced adhesion. In one study, truncation of 11 amino acids in the linker preferentially weakened binding at high force and high flow (14), whereas in the other study, the same truncation preferentially strengthened binding at low force and low flow (15). To understand the activation of VWF at the molecular level, it is necessary to not only understand how the N-terminal linker regulates A1 in flow or force but also to identify amino acids that are key to its function.

In the present study, we searched systematically for key amino acids in the N-terminal linker that are relevant to the binding function of the A1 domain. The results confirmed that the N-terminal linker has an inhibitory function, and a molecular mechanism behind this observation is presented. First, mutagenesis and flow chamber experiments were used to identify regions and amino acids of the N-terminal linker that activate A1 when deleted or mutated. These experiments showed that deleting or mutating Asp^{1261} into a non-negatively charged amino acid dramatically activated the A1 domain at any shear stress. Then molecular dynamics (MD) simulations were run to provide a structural explanation for how Asp^{1261} reduces binding of A1 to GpIbα. The model suggested by the simulations was then validated by further flow chamber experiments. Overall, this study shows how the specific interaction between Asp^{1261} in the N-terminal linker and the rest of A1 is crucial for the auto-regulatory function of this protein.

Results

Flow chamber experiments with different constructs

To identify key amino acids in the N-terminal linker that regulate binding, we measured binding of GpIbα to various truncated A1 domain constructs as follows. The A1 domain constructs were anchored to a surface through a C-terminal biotin tag, and the binding domain of GpIbα was anchored to microbeads via a C-terminal biotin tag. The beads were allowed to settle onto the surface, washed at 2 dyn/cm^2 fluidic wall shear stress, and then subjected to stepwise increasing or decreasing flow, whereas their movement was recorded with videomicroscopy. For the purpose of this manuscript, a wild-type construct is named A1_*n*, where *n* indicates the position of the N-terminal amino acid (*e.g.* A1_1238 denotes a A1 construct starting at position 1238 and thus containing the entire N-terminal linker). Constructs bearing a single-point mutation will be identified with A1_n_*x*, where *x* is the name of the particular mutation (*e.g.* D1261Q).

When surfaces were coated with the A1_1238 construct with the full N-terminal linker, the GpIbα-coated beads moved rapidly across surfaces (Fig. 2*a*) and detached as shear stress decreased (Fig. 2*b*). This shear-enhanced rolling adhesion is consistent with that observed previously for platelets of GpIbα-coated beads binding to isolated A1 domain with the full N-terminal linker (15, 14) and for full-length VWF (16). In comparison, when the surface was coated with the A1_1261 construct that contains only the last 11 amino acids of the N-terminal linker, beads rolled more slowly at all shear stresses (Fig. 2*a*). This indicates that the construct with the shorter linker mediated stronger adhesion, consistent with previous studies indicating that the first 23 N-terminal amino acids of the A1 domain that are present in A1_1238 but not in A1_1261 (Fig. 1) play an inhibitory function (6, 15).

Importantly, GpIbα-coated beads binding to immobilized A1_1261 still demonstrated shear-enhanced adhesion in which GpIbα beads detached below a shear threshold (Fig. 2*b*), demonstrating that the 23 amino acids between 1238 and 1261 were

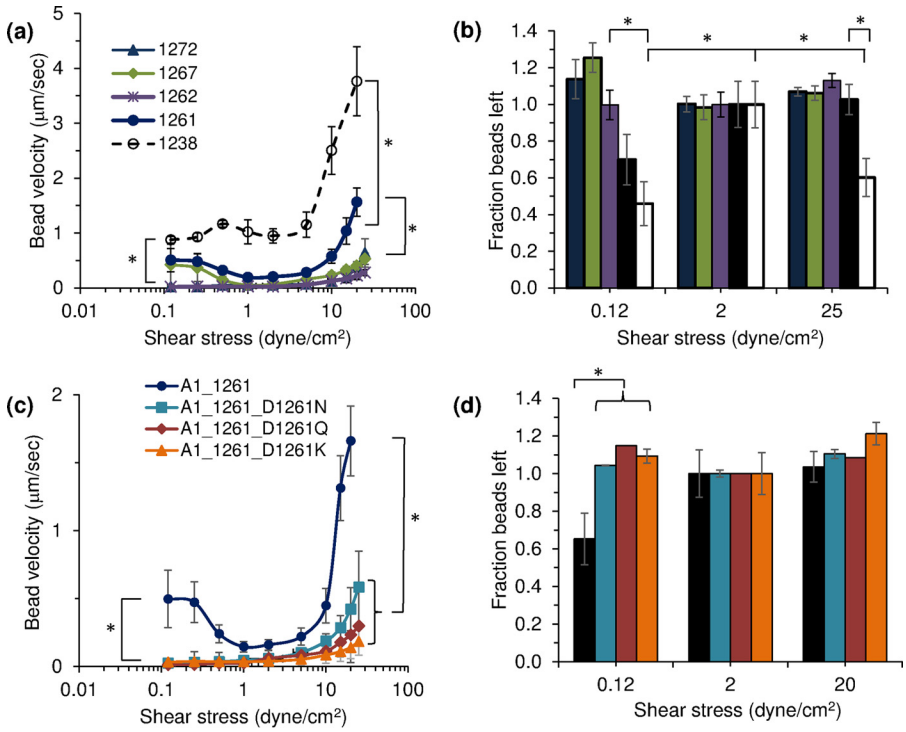

Figure 2. Flow chamber experiments with various constructs. *a–d*, the effect of various lengths (*a* and *b*) of the N-terminal linker and single-point mutations (*c* and *d*) in A1_1261 on the binding activity of A1 determined by measuring the rolling velocity of GpIbα beads as a function of shear stress (*a* and *c*) and by the fraction of beads that stay bound (can be larger than 1 because new beads can enter the field of view) under various shear stresses (*b* and *d*). The *error bars* represent the standard deviation of values from three independent experiments. An *asterisk* indicates that the difference between two values is statistically significant, *i.e.* $p < 0.05$. The *p* values were calculated from a one-tailed Student's *t* test. For simplicity, the statistical significance is indicated between groups of values. One exception is that at low shear, the velocity of beads rolling over A1_1272 (*green line*) is not different from the velocity of beads rolling over A1_1261 (*black line*) in *a*. This is due to an artifact in one of the experiments where new beads entered the field of view and were still counted. This was an isolated event, which could have been due to an unusually large concentration of injected beads, an inhomogeneous protein concentration on the plate, or a combination of the two.

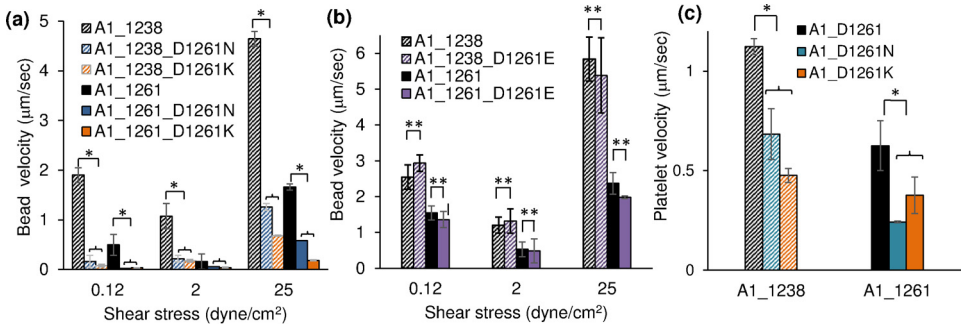

Figure 3. The key role of Asp^{1261}. Various single-point mutations of Asp^{1261} in the constructs A1_1238 (full N-terminal linker) and A1_1261 (shorter N-terminal linker) were examined. *a*, activating mutations of Asp^{1261} tested with GpIbα-coated beads. *b*, comparison between wild-type A1 and the D1261E mutants where the negative charge at position 1261 is conserved. *c*, activating mutations of Asp^{1261} tested with platelets rolling at 25 dyne/cm^2. The *error bars* represent the standard deviation of values from three independent experiments. An *asterisk* indicates that the difference between two values is statistically significant, *i.e.* $p < 0.05$ (calculated from a one-tailed Student's *t* test).

not needed for shear dependent adhesion in these studies. In contrast, GpIbα-coated beads were nearly stationary and did not detach at low flow when bound to the A1_1261, A1_1267, and A1_1272 constructs that contain 10 or fewer amino acids in the N-terminal linker (Fig. 2, *a* and *b*). These observations suggest that the aspartate at position 1261 might play a key role in the inhibition of binding between A1 and GpIbα and in shear-enhanced adhesion because its removal strongly activates binding and eliminates shear enhanced adhesion.

To determine why removal of residue 1261 is so critical, A1_1261 variants with single-point mutations were expressed in which the negatively charged aspartic acid at position 1261 was mutated into the neutral amino acids glutamine (D1261Q) or asparagine (D1261N) or the positively charged amino acid lysine (D1261K). All three variants supported adhesion with significantly lower bead-rolling velocities at low and high shear compared with A1_1261 (Fig. 2*c*) and with no detachment of beads at low flow (Fig. 2*d*). Similar results were observed when the D1261N and D1261K substitutions were introduced into A1_1238 with the longer linker (Fig. 3*a*). In contrast, when aspartic acid was replaced with glutamic acid to maintain the negative charge (D1261E), rolling velocities remained unchanged compared with wild-type A1 constructs with the same length N-terminal linker (Fig. 3*b*). Together, these results dem-

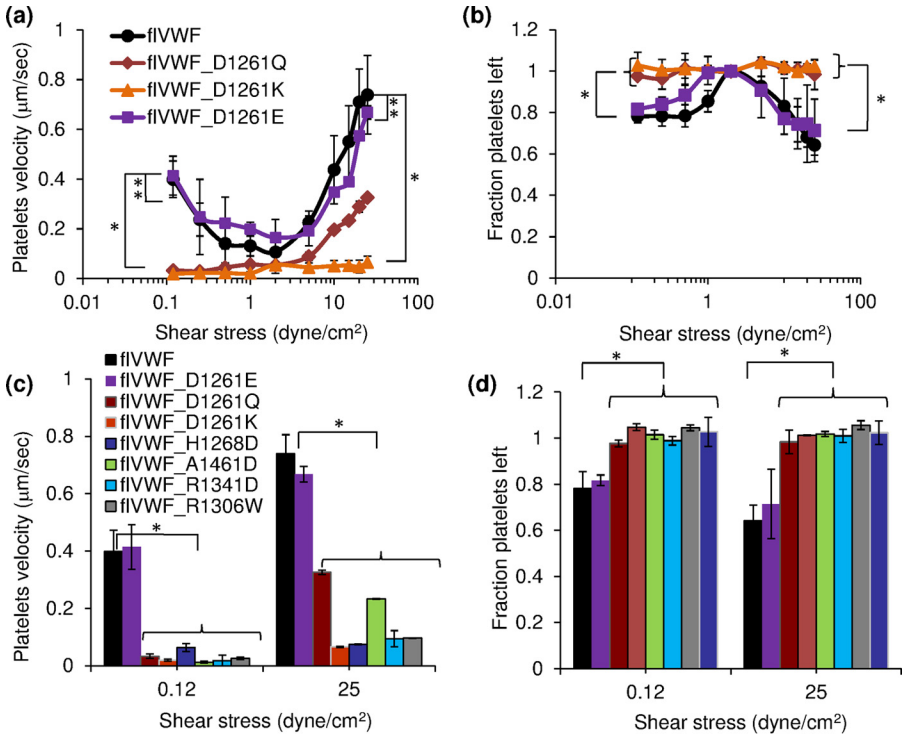

Figure 4. Flow chamber experiments with various constructs of full-length VWF. *a* and *b*, the effect of various single-point mutations of Asp^{1261} on the binding activity of the A1 domain in flVWF determined by measuring the bound velocity of platelets as a function of shear rate (*a*) and by the fraction of platelets that stay bound under various shear rates (*b*). *c* and *d*, comparison of single-point mutations of Asp^{1261} in the A1 domain of flVWF with clinically observed type 2B mutations based on the bound velocity of platelets (*c*) and the fraction of platelets that stay bound under various shear rates (*d*). The *error bars* represent the standard deviation of values from at least two independent experiments. An *asterisk* indicates that the difference between two values is statistically significant, i.e. $p < 0.05$ (calculated from a one-tailed Student's *t* test).

onstrate that the inhibitory function of the N-terminal linker involves ionic interactions between the residue at position 1261 and the rest of the bound complex.

To understand whether Asp^{1261} plays a key inhibitory role in a more physiological context, similar experiments were performed with blood platelets instead of GpIbα-coated beads. Again, the D1261N and D1261K mutations activated adhesion as indicated by a decrease in platelet rolling velocity (Fig. 3*c*). To test the importance of Asp^{1261} in full-length VWF (flVWF), we expressed recombinant multimeric flVWF with various mutations at position 1261. The two variants with a negative charge at position 1261 (wild-type flVWF and flVWF_D1261E) mediated nearly identical shear-enhanced rolling adhesion of platelets (Fig. 4, *a* and *b*), whereas variants with a neutral charge (D1261Q) or a positive charge (D1261K) at position 1261 mediated strong stationary binding to blood platelets even at low flow (Fig. 4, *a* and *b*). These results indicate the importance of the negative charge at position 1261 for regulating platelet adhesion to VWF.

Finally, we asked whether the change in binding strength caused by elimination of Asp^{1261} is likely to be physiologically relevant by comparing these engineered mutations to several mutations that are associated with type 2B von Willebrand disease, a bleeding disorder in which VWF binding to platelets is enhanced, leading to depletion of its largest multimers from the blood (17). Variants of flVWF with neutral (D1261Q) or positive (D1261K) charge at residue 1261 mediated binding with similar level of activation as flVWF variants with the following reported type 2B mutations: H1268D, A1461D, R1341D, and R1306W (Fig. 4, *c* and *d*). This indicates that the inhibitory function of Asp^{1261} in the A1 domain is of crucial importance to prevent the pathological activation of VWF.

Inhibitory function of Asp^{1261} investigated by simulations and mutagenesis

To investigate the inhibitory function of Asp^{1261} at a structural level, MD simulations were run with the complex between A1 and GpIbα. Two simulations were performed using wild-type A1_1261 and two using the single-point mutant A1_1261_D1261K. The A1–GpIbα complex was derived from the X-ray structure crystallized with the snake venom botrocetin (the latter was removed) because this is the only available X-ray structure of the complex where electron density for the N-terminal linker of A1 is visible starting at position 1261 (see "Materials and methods" for details about the setup). However, the structure used here is very similar to the complex between A1 and GpIbα crystallized without botrocetin except that in the latter, the N-terminal linker is visible starting only at residue 1269; after superimposition, the C_α root mean square deviation (RMSD) of those residues visible in both structures was 1.25 Å.

In all four simulations, the A1–GpIbα complex was stable as indicated by the RMSD from the initial structure (supplemental Fig. S1), which is consistent with previous MD studies (18). The individual proteins GpIbα and A1 showed even less flexibility, whereas the core A1 domain (defined as residues 1272–1461) was most stable (supplemental Fig. S1). Salt bridge analysis revealed that in wild-type A1 Asp^{1261} engaged in salt bridges with some positively charged side chains in core A1, *i.e.* Arg^{1308},

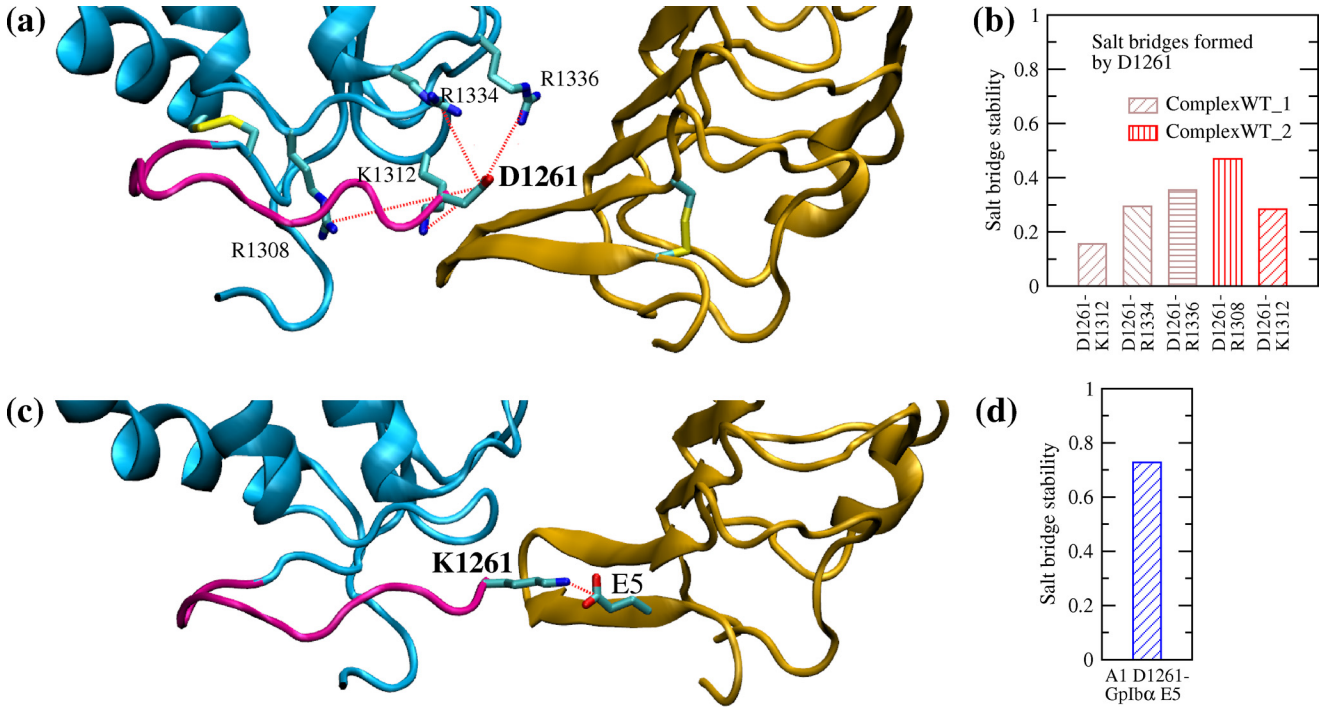

Figure 5. Salt bridge analysis from MD simulations. *a* and *c*, salt bridges involving Asp[1261] formed in at least 10% of the simulation frames during one of two runs with the wild-type complex (*a*) and the complex bearing the mutation D1261K (*c*). *b* and *d*, the plots show the frequency of salt bridge formation during the simulations with the wild-type (*b*) and the mutant (*d*), respectively.

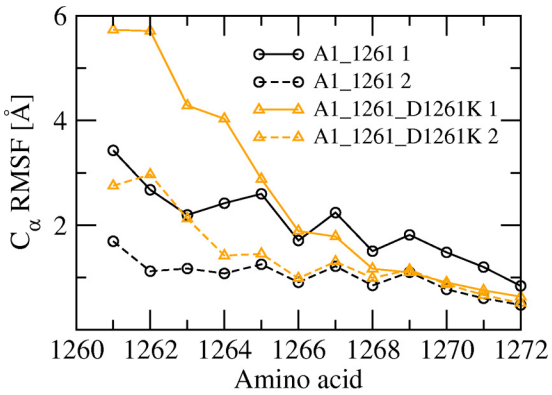

Figure 6. C_α RMSF calculated from the last 40 ns of in total 50-ns-long simulations with the wild-type and mutant structure. Shown is only the RMSF of amino acids in the N-terminal linker.

Lys[1312], Arg[1334], and Arg[1336] (Fig. 5, *a* and *b*). However, in the simulations with the single-point mutant D1261K, Lys[1261] did not form salt bridges with any residues located in core A1. Instead, in one run it formed a stable salt bridge with Glu[5] of GpIbα (Fig. 5, *c* and *d*), whereas in the other run the N-terminal linker was very flexible, as indicated by the root mean square fluctuations (RMSF) of C_α atoms (Fig. 6), and consequently Lys[1261] did not significantly engage in salt bridge formation with either GpIbα or the A1 core domain.

The differing patterns of salt bridge formation between aspartate and lysine at position 1261 suggested two contrasting hypotheses why A1_1261_D1261K is much more active in binding to GpIbα than A1_1261. One explanation could be that Lys[1261] forms a stable salt bridge with Glu[5] in GpIbα, thus providing an additional interaction between the two proteins, which is not possible with wild-type A1 where an aspartate is present at position 1261. Another plausible explanation is that Asp[1261] forms salt bridges with core A1, thus anchoring the N-terminal linker in such a way that it can interfere with the bond with GpIbα. Experimental evidence that mutations of Asp[1261] to neutral residues also activate the A1 domain suggests that the disruption of salt bridges with core A1 is likely the major mechanism.

To validate the role of salt bridge interactions in anchoring the N-terminal linker and inhibiting the A1 domain, variants with single-point mutations were expressed where the positively charged residues at positions 1308, 1312, 1334, and 1336 were mutated to aspartate. These amino acids were observed in the simulations to form salt bridges with Asp[1261] (Fig. 5*a*), so mutation of these residues is expected to activate the A1 domain. In addition, the single-point mutant K1371D was also expressed as a negative control because the residue at this position does not interact with the N-terminal linker but forms a salt bridge with GpIbα (Fig. 7, *a* and *b*). As predicted, the mutations R1308D and R1336D enhanced the binding activity of the A1 domain at low and high shear, as shown by the decreased rolling velocity (Fig. 8*a*) and decreased bead detachment (Fig. 8*b*) compared with the wild-type. The mutations K1312D and R1334D and the negative control K1371D inhibited the adhesive function of the A1 domain (Fig. 8*b*). All three of these residues formed salt bridges with residues in GpIbα in simulations performed with complexes from multiple crystal structures; Arg[1334] and Lys[1371] formed stable salt bridges with GpIbα in both the simulations described here (Fig. 7, *a* and *b*) and those described in earlier studies (18), whereas Lys[1312] formed salt bridges with Glu[5] or Glu[14] in earlier simulations only (Fig. 7*c*) (18). Remarkably, the earlier simulations were performed with crystal structures in which no electron density was visible for residue Asp[1261] (PDB codes 1SQ0 and

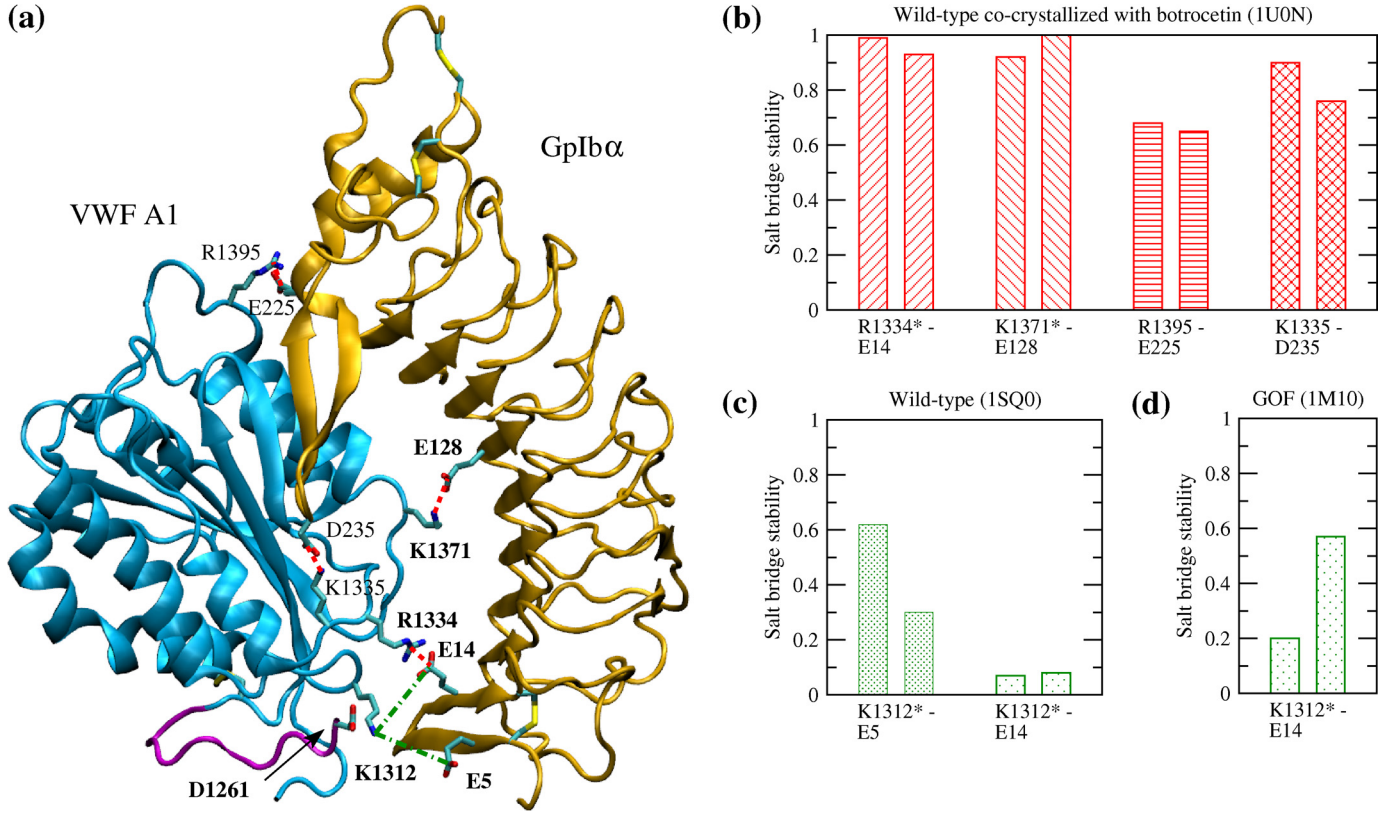

Figure 7. Interprotein salt bridges. *a*, interprotein salt bridges that are observed in at least 60% of the frames of the simulations presented here are shown by *red dashed lines*. The salt bridges between Lys^{1312} in A1 and two glutamic acids in GpIbα were not observed here but in previously published simulations started from complexes containing a shorter A1 N-terminal linker (18) (PDB codes 1SQ0 and 1M10) and thus are highlighted by a *green dash-dotted line*. Amino acids in A1 that are mutated in the flow chamber experiments are indicated in *bold type* and so are the residues in GpIbα with which they form salt bridges. The side chain of Asp^{1261} is shown for reference. *b*, fraction of frames where a salt bridge is observed to be formed (using the last 40 ns of in total 50-ns-long simulations) in both runs with the wild-type complex presented here. *c* and *d*, formation of interprotein salt bridges involving Lys^{1312} observed in previously published simulations started from a complex with a shorter N-terminal linker (PDB code 1SQ0) and from a complex containing gain-of-function (*GOF*) mutations that are clinically associated with type 2B von Willebrand disease (PDB code 1M10), respectively (18). The *asterisk* next to an amino acid number indicates that it is mutated in flow chamber experiments thus removing the salt bridge. The PDB codes of the structures used to start the simulations here (1U0N) and in a previous publication (18) (1SQ0 and 1M10) are indicated for each plot. See "Materials and methods" for the definition of a salt bridge.

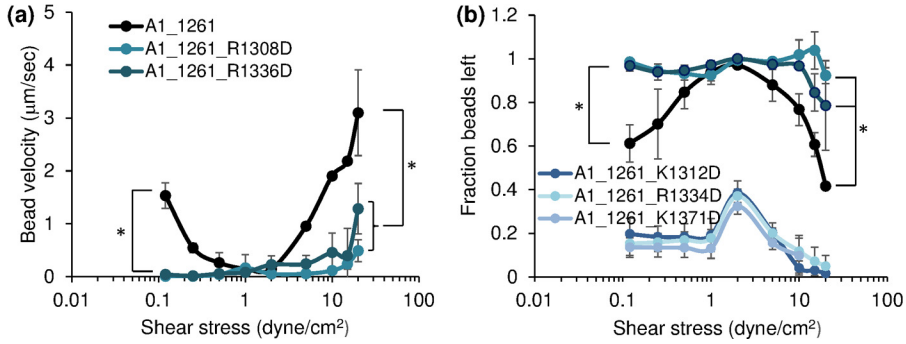

Figure 8. Validation of the anchoring mechanism of the N-terminal linker through salt bridges. *a* and *b*, velocity (*a*) and ratios (*b*) of beads during flow chamber experiments with variants of A1 bearing single-point mutations that eliminate specific salt bridge interactions. The *error bars* represent the standard deviation of values from three independent experiments. An *asterisk* indicates that the difference between two values is statistically significant, *i.e.* $p < 0.05$ (calculated from a one-tailed Student's *t* test).

1M10), suggesting that Lys^{1312} is only able to form salt bridges with GpIbα when it is not forming a salt bridge with Asp^{1261}.

In summary, salt-bridge interactions are key to regulate binding between A1 and GpIbα. Mutation of positively charged amino acids that form a salt bridge with Asp^{1261} but not with GpIbα activates binding. However, mutating positively charged residues that interact with GpIbα inhibits binding whether or not they also interact with Asp^{1261}. This indicates that the destabilizing effect of abrogating an intermolecular interaction is larger than the activation because of removal of the inhibitory effect of the N-terminal linker. The observation that Lys^{1312} is not observed to form a salt bridge with both GpIbα and Asp^{1261} simultaneously also suggests a mechanism by which Asp^{1261} and the N-terminal linker may inhibit GpIbα binding.

Discussion

The recruitment of blood platelets to the site of vascular injury during hemostasis is mediated by the binding of the A1 domain of VWF to platelet surface receptors, and it is particularly essential under high shear conditions. Under normal blood flow conditions, the A1 domain is not active, and this has been largely attributed to the inhibitory function of its N-terminal linker (16, 15). However, the exact molecular mechanism has not been elucidated by which the N-terminal linker prevents binding of A1 to GpIbα under low flow conditions and is involved in high-shear activation of A1 binding to GpIbα. Using a combination of flow chamber experiments and MD simulations, the present study investigated the role of key amino acids in the N-terminal linker in regulating the adhesive function of the A1 domain. Four main conclusions arise from the results. First, Asp^{1261} is the most critical residue for the inhibitory function of the N-terminal linker (Figs. 2 and 3). Second, Asp^{1261} is critical for shear-enhanced adhesion (Figs. 2 and 3). Third, Asp^{1261} inhibits the A1 domain because it forms salt bridges with positively charged residues in the rest of the protein (Fig. 5). Fourth, interprotein salt bridges between A1 and GpIbα are necessary for the stability of the complex (Figs. 7 and 8). Overall, the present study indicates that interactions between charged residues are key to the regulation of the A1 domain either through anchoring of the N-terminal linker to the rest of A1 and inhibiting binding or by stabilizing the complex between A1 and GpIbα.

A major impediment to understanding the structural basis of the N-terminal linker inhibition has been that residues 1238–1260 have been considered essential to the inhibitory function of the linker (14, 15) but are not included in any crystal structures of A1. However, we established here that the short N-terminal linker (residues 1261–1270) is sufficient for inhibition and shear-enhanced adhesion (Fig. 2), although residues 1238–1260 indeed amplify these effects. Thus, we can directly evaluate the structural mechanism of inhibition from the crystal structure of the A1–GpIbα complex in which the short linker is fully resolved (PDB code 1U0N) (8). Both crystal structure (8) and our simulations (Fig. 7) clearly demonstrate that the short linker and GpIbα can simultaneously bind stably to A1, so the short linker is not a competitive inhibitor of GpIbα. However, the linker and GpIbα bind to overlapping sites on A1 that include Lys^{1312} (Fig. 7). This demonstrates that the N-terminal linker acts as a *parasteric inhibitor*, which is defined as a noncompetitive inhibitor that binds to a site on a receptor that overlaps with the ligand (19). The parasteric mechanism of the N-terminal linker may be reminiscent of toehold nucleic acid strand displacement, in which single-stranded nucleic acid binds to an exposed single-stranded toehold on double-stranded nucleic acid, allowing rapid sequential displacement of the original and otherwise stable complex. That is, we propose that the linker docks to A1 in the A1–GpIbα complex and then disrupts the salt bridges between Lys^{1312} and GpIbα, which are essential to binding function (Fig. 8).

This proposed mechanism of parasteric inhibition of GpIbα by the N-terminal linker provides a structural explanation for multiple observations about the biophysics of the interaction between VWF and GpIbα. First, it is known that stretching of VWF in flow activates binding to GpIbα. This stretching would extend both N- and C-terminal linkers away from A1, which would dislodge Asp^{1261}, unmasking the full GpIbα binding site on A1. Second, the complex between A1 and GpIbα is known to form catch bonds that are longer lived under increased tensile force (9). Because GpIbα can bind to core A1 simultaneously as the N-terminal linker, A1 and GpIbα can transiently bind to each other even when the N-terminal linker is still docked in place. At that point, tensile force transmitted through the complex would pull away the N-terminal linker, unmasking Lys^{1312} to strengthen the A1–GpIbα complex. It should not matter whether force is transmitted primarily through the C or N terminus in this model, because MD simulations showed that in both cases, the disulfide bond linking the two terminii of the A1 domain moves away from GpIbα (18). Third, the A1–GpIbα complex displays two distinct lifetimes (14, 20). In the short-lived state, Asp^{1261} would be fully docked, forming a salt bridge to Lys^{1312}, whereas in the long-lived state, Asp^{1261} would be dislodged, and Lys^{1312} would form salt bridges with GpIbα. Fourth, this mechanism explains why no allosteric conformational changes have been observed in the core A1 domain between various crystallographic structures of the A1 domain in isolation (5), in complex with GpIbα (8, 21) or bearing clinically known gain-of-function mutations (22, 23), despite many observations that might otherwise suggest allosteric regulation.

The inhibitory mechanism of the N-terminal linker described here might also explain how some naturally occurring mutations lead to type 2B von Willebrand disease, a bleeding disorder caused by depletion of the hemostatically most active large multimers of VWF caused by their clearance by platelets (17). Type 2B mutations R1308C (24) and R1308P would eliminate a positive charge that helps anchor the N-terminal linker (Fig. 5*b*). Type 2B mutations R1306W/Q/L, I1309V, S1310F, W1313C, and R1341W/Q/P/L are also located in the vicinity where the N-terminal linker docks, and P1266L/Q, H1268N/D, and C1272G are in the N-terminal linker where it docks to A1. Therefore, these type 2B mutations may also activate platelet binding by destabilizing the linker from the docked position where it inhibits GpIbα binding.

In conclusion, the present study highlights that salt bridges are a key component for the binding function of the A1 domain and its regulation. Intermolecular salt bridges stabilize the complex between A1 and GpIbα, whereas the N-terminal linker of A1 destabilizes the complex, in large part because of salt bridges between Asp^{1261} and the core of the A1 domain. Because the N-terminal linker and GpIbα can bind simultaneously to the core of the A1 domain yet have overlapping binding sites, they act as noncompetitive parasteric inhibitors of each other. The results presented here provide a structural explanation for many prior observations about the regulation of the complex, including its mechanical activation (9), dual lifetimes (14, 20), and the existence of activating type 2B von Willebrand disease mutations (17). The present work also strongly suggests that the N-terminal linker can induce detachment of the A1–GpIbα complex and thus could provide a novel mechanism to dissolve thrombi. More generally, design of novel anti-thrombotic drugs that target the VWF–GpIbα interaction should take into account the role of charged interactions.

Materials and methods

Construction of expression plasmids for VWF A1 domain wild-type and mutants

The DNA fragments containing A1_1261 or A1_1238 were first obtained by PCR amplification using the full-length human VWF cDNA plasmid as a template and corresponding primers that included a NheI site at the 5′ end and a XhoI site at the 3′ end of the A1 domain. All inserted A1 domain constructs ended at position 1472. The amplified fragments were then cloned by TA cloning into the vector pCR2.1-TOPO following the protocols provided by the manufacturer (Invitrogen). The single-site mutations D1261K, D1261N, and D1261Q in A1_1261 and A1_1238, respectively, and the deletion mutations in A1_1261 to generate the constructs A1_1261, A1_1267, and A1_1272 were introduced into the corresponding wild-type A1 fragments according to the protocol of the QuikChange site-directed mutagenesis kit (Stratagene, La Jolla, CA). The desired DNA sequences of the wild-type and various mutant A1 fragments were confirmed by DNA sequencing. By taking advantage of the NheI and XhoI restriction sites on the vector, these A1 DNA fragments were further subcloned into the pBIG expression vector in frame with four repeats of GGGGS linker between the C terminus of the A1 domain and a Biotin tag. The resulting sequence of the expressed protein was therefore MPSSVSWGILLLAGLCCLVPVSLA↓ERAS (VWF insert) LEGRLNDIFEAQKIEWH, with the arrow indicating the location at which the signal peptide is cleaved, so that the secreted protein starts just after this.

Expression of various recombinant VWF A1 domain proteins

The recombinant expression constructs were transiently transfected into CHO Tet-On cells with Lipofectamine 2000 (Invitrogen) for protein expression. The expression was induced by doxycycline (2 μg/ml) in the presence of biotin (50 μM) in DMEM culture medium (Invitrogen) with 10% tetracycline-free fetal bovine serum (Atlanta Biologicals, Lawrenceville, GA) for 72 h before harvest. Culture medium containing secreted recombinant A1 protein was collected and concentrated five times using an Amicon Ultra-15 centrifugal filters (EMD Millipore, Billerica, MA). Free biotin was removed from the samples using a desalting PD-10 column (GE Healthcare).

Expression of recombinant full-length VWF

The cDNA containing full-length VWF, wild type, or mutants, in the pBIG vector (25) was transiently transfected into HEK293 Tet-On cells (Clontech) with Lipofectamine 2000 (Invitrogen). Proteins were expressed for 48 h in serum-free FreeStyle 293 medium (Life Technologies) in the presence of 2 μg/ml of doxycycline and 50 μM biotin. The culture medium containing secreted VWF was concentrated, and the free biotin was removed as described above.

Preparation of surfaces with VWF constructs

VWF constructs were anchored to surfaces via the biotin tag as follows. 35-mm tissue culture polystyrene dishes were incubated with a 100-μl droplet of 200 μg/ml biotin-BSA for 2 h at 37 °C, washed three times with 0.2% BSA-PBS (w/v), incubated with 100 μg/ml streptavidin for 30 min at 37 °C, washed three times with 0.2% BSA-PBS (w/v), and incubated overnight at 4 °C in 0.2% PBS-BSA. The dishes were then incubated for 30 min at 37 °C with a solution containing the biotinylated VWF A1 or full-length VWF prepared as described above, washed three times with 0.2% BSA-PBS (w/v), and blocked with 0.2% BSA-PBS (w/v). The amount of biotinylated VWF used in this surface functionalization was determined to be sufficient to saturate the available biotin-binding sites by using biotin-4-fluorescin to test for the presence of free biotin-binding sites using the method of Kada *et al.* (26). Briefly, flat bottomed 96-well dishes were functionalized with biotin-BSA and streptavidin as described above and shown to quench up to 25 nM of biotin-4-fluorescein in 100 μl. This indicates the availability of binding sites for 2 pmol biotin on the streptavidin-functionalized surfaces. After incubation with biotinylated VWF, the surfaces displayed essentially the same (unquenched) fluorescence as control dishes with no streptavidin, indicating that all biotin-binding sites were now saturated. Given an expected functionalized surface area of 32 mm^2 in the wells, 2 pmol translates to a site density of two biotin-binding sites per 50 nm^2 area, consistent with the size of streptavidin tetramers and the expectation that two biotin-binding sites will be free because they face upward away from the biotin-BSA layer on the surface. A 3-fold excess of this amount of biotinylated VWF was used to functionalize the 35-mm dishes for insurance in case the droplet used in the flow chamber had a slightly larger surface area than in the dishes.

Preparation of washed platelets

The platelets were isolated from the blood of healthy donors, which had been drawn into acid citrate dextrose tubes. The platelets were separated by differential centrifugation in the presence of apyrase and PGE-1 (to inhibit platelet activation) and resuspended in Hepes Tyrodes buffer containing 0.1% BSA (27).

Preparation of GPIbα-coated microspheres

The N-terminal domain of GPIbα (amino acids 1–300 of the extracellular domain of GPIbα with a C-terminal biotin tag for oriented anchoring) was made using a previously described expression vector (28) and expressed in CHO cells. After desalting and concentrating via ammonium sulfate precipitation, the GC300 was bound to 3-μm-diameter streptavidin-coated Dynabeads (Invitrogen) with gentle mixing for 30 min at room temperature. The beads were then washed and resuspended in PBS with 0.1% BSA (w/v) for use in the flow chamber.

Platelet and microsphere adhesion in flow

Platelet adhesion studies were performed in a Glycotech™ parallel plate flow chamber as previously described (29), using functionalized 35-mm dishes prepared as described above as the lower surface. A 300-μl bolus of washed platelets or GPIbα-coated microspheres was introduced into a flow chamber and allowed to settle for 30 s, before PBS-BSA buffer was pushed through the chamber at the indicated shear stress and platelets or microspheres observed with a 10× objective and CCD camera. To calculate the velocity of platelets or microspheres at each shear stress, time-lapse videos were taken with a 10× objec-

Table 1
Simulation systems
The initial assignment of velocities was varied to make sure that simulations with the same construct sample a different conformational space.

Name	Construct	Temperature	Length
		K	*ns*
Complex WT_1	A1_1261/GpIbα	300	50
Complex WT_2	A1_1261/GpIbα	300	50
Complex D1261K_1	A1_1261_D1261K/GpIbα	300	50
Complex D1261K_2	A1_1261_D1261K/GpIbα	300	50

tive using MetaMorph or MicroManager software, at 1 frame/s, and the platelets or microspheres in the videos tracked using SVCell RS (DRVision Technologies, Bellevue, WA). The tracks were processed using MATLAB scripts to calculate the velocity of each platelet or microsphere at each time point. If the velocity in any frame was equal to or greater than the hydrodynamic velocity (particle radius times the shear rate or the estimated velocity of fluid at the midpoint of a platelet or microsphere touching the surface), then the platelet or microsphere was assumed to not be bound at that time point. The average velocity of all bound platelets or microspheres was calculated at each time point, and this value was averaged over all time points at a given shear stress to calculate the translocation velocity at a given shear stress.

Initial conformations for the MD simulations

To generate the initial conformations, the crystallographic structure with PDB code 1U0N was used, which contains the triplex between the A1 domain, GpIbα, and the snake venom botrocetin (8). The reason why this X-ray structure was chosen *versus* the one consisting of only A1 and GpIbα (PDB code 1SQ0) is that in the former the A1 domain contains a longer N-terminal linker, and in particular its N-terminal residue at position 1261 is of particular relevance for this manuscript. Botrocetin was deleted from the PDB file, and the resulting structure of the A1–GpIbα complex was then subjected to 200 steps of steepest descent minimization *in vacuo* using the program CHARMM (30) to relieve any possible strain in the system. The conformation with the single-point mutation D1261K was created per analogy from the wild-type using internal coordinates for the lysine side chain contained in the PARAM22 parameter set (31). The different simulations systems are summarized in Table 1.

Simulation setup

The MD simulations were performed with the program NAMD (32) using the CHARMM all-hydrogen force field (PARAM22) (31) with the CMAP extension (33, 34). The proteins were inserted into a cubic water box with side length of 110 Å, resulting in a system with a total of ~127,000 atoms. Chloride and sodium ions were added to neutralize the system and approximate a salt concentration of 150 mM. The water molecules overlapping with the protein or the ions were removed if the distance between the water oxygen and any atom of the protein or any ion was smaller than 3.1 Å. To avoid finite size effects, periodic boundary conditions were applied. After solvation, the system underwent 500 steps of minimization, whereas the coordinates of the heavy atoms of the protein were held fixed and subsequent 500 steps with no restraints. Each simulation was started with different initial random velocities to ensure that different trajectories were sampled whenever starting with the same initial state. Electrostatic interactions were calculated within a cutoff of 10 Å, whereas long-range electrostatic effects were taken into account by the particle mesh Ewald summation method (35). van der Waals interactions were treated with the use of a switch function starting at 8 Å and turning off at 10 Å. The dynamics were integrated with a time step of 2 fs. The covalent bonds involving hydrogens were rigidly constrained by means of the SHAKE algorithm with a tolerance of 10^{-8}. Snapshots were saved every 10 ps for trajectory analysis.

Before production runs, harmonic constraints were applied to the positions of all heavy atoms of the protein to equilibrate the system at 300 K during a time length of 0.2 ns. For those systems containing single-point mutations, harmonic constraints were kept on all heavy atoms except those of the mutated amino acid and of amino acids for which any side chain atom was within 4 Å of any side chain atom of the mutated residue (these were Lys^{1261}, Ile^{1261}, Ser^{1263}, Lys^{1312}, and Glu^{5} in GpIbα), and equilibration was continued for another 2 ns. After this equilibration phase, the harmonic constraints were released. The systems were simulated for in total 50 ns, and the first 10 ns of unconstrained simulation time were also considered part of the equilibration and were thus not used for the analysis. During both the equilibration and production phases, the temperature was kept constant at 300 K by using the Langevin thermostat (36) with a damping coefficient of 1 ps^{-1}, whereas the pressure was held constant at 1 atm by applying a pressure piston (37). The C_α RMSD calculated along the trajectories fluctuated ~2 Å for the entire complex in all simulations except in complex D1261K_1, in which the N-terminal linker was flexible (supplemental Fig. S1). This indicates that the simulations have likely converged and sampled conformational space around the bound state.

Determination of salt bridge formation

The trajectories were screened for the presence of salt bridges between Asp^{1261} or Lys^{1261}, respectively, and any other charged residue of A1 or GpIbα. An interaction was defined as salt bridge if the atoms N_ζ of Lys or C_ζ of Arg were closer than 4 or 5 Å, respectively, from either the C_γ of Asp or C_δ of Glu. All histidines were assumed neutral. Only salt bridges present in at least 10% of the simulation frames were considered for the analysis.

Author contributions—G. I., O. Y., and W. E. T. conceived and coordinated the study. G. I. performed and analyzed the simulations, interpreted the results, provided input into experimental design, and wrote the paper. O. Y. performed and analyzed the experiments. A.-Y. T. engineered and expressed VWF constructs. J. H. and J. L. expressed and purified full-length VWF. W. E. T., J. A. L., and J. C. provided input into experimental design and interpreted the results, and W. E. T. and J. A. L. critically revised the article. All authors reviewed the results and approved the final version of the manuscript.

Acknowledgments—We thank Dominic Chung for helpful and interesting discussions and John Kulman for providing the pBIG expression vector. The simulations were performed on the Ranger supercomputer at the Texas Advanced Computing Center thanks to an allocation on the Extreme Science and Engineering Development Environment with Grant TG-MCB060069N, which is made available in part through support from the National Science Foundation.

References

1. Savage, B., Saldívar, E., and Ruggeri, Z. M. (1996) Initiation of platelet adhesion by arrest onto fibrinogen or translocation on von Willebrand factor. *Cell* **84,** 289–297
2. Savage, B., Shattil, S. J., and Ruggeri, Z. M. (1992) Modulation of platelet-function through adhesion receptors: a dual role for glycoprotein-IIb-IIIa (integrin-$\alpha_{IIb}\beta_3$) mediated by fibrinogen and glycoprotein-Ib-von Willebrand factor. *J. Biol. Chem.* **267,** 11300–11306
3. Miyata, S., Goto, S., Federici, A. B., Ware, J., and Ruggeri, Z. M. (1996) Conformational changes in the A1 domain of von Willebrand factor modulating the interaction with platelet glycoprotein Ibα. *J. Biol. Chem.* **271,** 9046–9053
4. Peterson, D. M., Stathopoulos, N. A., Giorgio, T. D., Hellums, J. D., and Moake, J. L. (1987) Shear-induced platelet-aggregation requires vonwillebrand-factor and platelet membrane glycoprotein-Ib and glycoprotein-IIb-IIIa. *Blood* **69,** 625–628
5. Emsley, J., Cruz, M., Handin, R., and Liddington, R. (1998) Crystal structure of the von Willebrand factor A1 domain and implications for the binding of platelet glycoprotein Ib. *J. Biol. Chem.* **273,** 10396–10401
6. Sugimoto, M., Dent, J., McClintock, R., Ware, J., and Ruggeri, Z. (1993) Analysis of structure-function relationships in the platelet membrane glycoprotein Ib-binding domain of von Willebrand's factor by expression of deletion mutants. *J. Biol. Chem.* **268,** 12185–12192
7. Miyata, S., and Ruggeri, Z. M. (1999) Distinct structural attributes regulating von Willebrand factor A1 domain interaction with platelet glycoprotein Iba under flow. *J. Biol. Chem.* **274,** 6586–6593
8. Fukuda, K., Doggett, T., Laurenzi, I. J., Liddington, R. C., and Diacovo, T. G. (2005) The snake venom protein botrocetin acts as a biological brace to promote dysfunctional platelet aggregation. *Nat. Struct. Mol. Biol.* **12,** 152–159
9. Yago, T., Lou, J., Wu, T., Yang, J., Miner, J. J., Coburn, L., López, J. A., Cruz, M. A., Dong, J.-F., McIntire, L. V., McEver, R. P., and Zhu, C. (2008) Platelet glycoprotein Ibα forms catch bonds with human WT vWF but not with type 2B von Willebrand disease vWF. *J. Clin. Invest.* **118,** 3195–3207
10. Yakovenko, O., Sharma, S., Forero, M., Tchesnokova, V., Aprikian, P., Kidd, B., Mach, A., Vogel, V., Sokurenko, E., and Thomas, W. E. (2008) FimH forms catch bonds that are enhanced by mechanical force due to allosteric regulation. *J. Biol. Chem.* **283,** 11596–11605
11. Guo, B., and Guilford, W. H. (2006) Mechanics of actomyosin bonds in different nucleotide states are tuned to muscle contraction. *Proc. Natl. Acad. Sci. U.S.A.* **103,** 9844–9849
12. Konstantopoulos, K., Hanley, W. D., and Wirtz, D. (2003) Receptor-ligand binding: 'catch' bonds finally caught. *Curr. Biol.* **13,** R611–R613
13. Xiao, T., Takagi, J., Coller, B. S., Wang, J. H., and Springer, T. A. (2004) Structural basis for allostery in integrins and binding to fibrinogen-mimetic therapeutics. *Nature* **432,** 59–67
14. Ju, L., Dong, J.-F., Cruz, M. A., and Zhu, C. (2013) The N-terminal flanking region of the A1 domain regulates the force-dependent binding of von Willebrand factor to platelet glycoprotein Ibα. *J. Biol. Chem.* **288,** 32289–32301
15. Tischer, A., Cruz, M. A., and Auton, M. (2013) The linker between the D3 and A1 domains of vWF suppresses A1-GPIb catch bonds by site-specific binding to the A1 domain. *Protein Sci.* **22,** 1049–1059
16. Doggett, T. A., Girdhar, G., Lawshe, A., Miller, J. L., Laurenzi, I. J., Diamond, S. L., and Diacovo, T. G. (2003) Alterations in the intrinsic properties of the GPIbα-VWF tether bond define the kinetics of the platelet-type von Willebrand disease mutation, Gly233Val. *Blood* **102,** 152–160
17. Ruggeri, Z. M., Pareti, F. I., Mannucci, P. M., Ciavarella, N., and Zimmerman, T. S. (1980) Heightened interaction between platelets and factor-VIII-von Willebrand Factor in a new subtype of von Willebrand's disease. *N. Engl. J. Med.* **302,** 1047–1051
18. Interlandi, G., and Thomas, W. (2010) The catch bond mechanism between von Willebrand factor and platelets investigated by molecular dynamics simulations. *Proteins* **78,** 2506–2522
19. Kisiela, D. I., Avagyan, H., Friend, D., Jalan, A., Gupta, S., Interlandi, G., Liu, Y., Tchesnokova, V., Rodriguez, V. B., Sumida, J. P., Strong, R. K., Wu, X.-R., Thomas, W. E., and Sokurenko, E. V. (2015) Inhibition and reversal of microbial attachment by an antibody with parasteric activity against the FimH adhesin of uropathogenic *E coli*. *PLoS Pathog.* **11,** e1004857
20. Kim, J., Zhang, C.-Z., Zhang, X., and Springer, T. A. (2010) A mechanically stabilized receptor-ligand flex-bond important in the vasculature. *Nature* **466,** 992–995
21. Dumas, J. J., Kumar, R., McDonagh, T., Sullivan, F., Stahl, M. L., Somers, W. S., and Mosyak, L. (2004) Crystal structure of the wild-type von Willebrand factor A1-glycoprotein Ibα complex reveals conformation differences with a complex bearing von Willebrand disease mutations. *J. Biol. Chem.* **279,** 23327–23334
22. Celikel, R., Ruggeri, Z. M., and Varughese, K. I. (2000) von Willebrand factor conformation and adhesive function is modulated by an internalized water molecule. *Nat. Struct. Biol.* **7,** 881–884
23. Huizinga, E. G., Tsuji, S., Romijn, R. A., Schiphorst, M. E., de Groot, P. G., Sixma, J. J., and Gros, P. (2002) Structures of glycoprotein Ibα and its complex with von Willebrand factor A1 domain. *Science* **297,** 1176–1179
24. Randi, A. M., Rabinowitz, I., Mancuso, D. J., Mannucci, P. M., and Sadler, J. E. (1991) Molecular basis of von Willebrand disease type-IIB: Candidate mutations cluster in one disulfide loop between proposed platelet glycoprotein-Ib binding sequences. *J. Clin. Invest.* **87,** 1220–1226
25. Chung, D. W., Chen, J., Ling, M., Fu, X., Blevins, T., Parsons, S., Le, J., Harris, J., Martin, T. R., Konkle, B. A., Zheng, Y., and López, J. A. (2016) High-density lipoprotein modulates thrombosis by preventing von Willebrand factor self-association and subsequent platelet adhesion. *BLOOD* **127,** 637–645
26. Kada, G., Falk, H., and Gruber, H. (1999) Accurate measurement of avidin and streptavidin in crude biofluids with a new, optimized biotin-fluorescein conjugate. *Biochim. Biophys. Acta* **1427,** 33–43
27. Goto, S., Salomon, D. R., Ikeda, Y., and Ruggeri, Z. M. (1995) Characterization of the unique mechanism mediating the shear-dependent binding of soluble von Willebrand factor to platelets. *J. Biol. Chem.* **270,** 23352–23361
28. Kulman, J. D., Satake, M., and Harris, J. E. (2007) A versatile system for site-specific enzymatic biotinylation and regulated expression of proteins in cultured mammalian cells. *Protein Expr. Purif.* **52,** 320–328
29. Thomas, W. E., Trintchina, E., Forero, M., Vogel, V., and Sokurenko, E. V. (2002) Bacterial adhesion to target cells enhanced by shear force. *Cell* **109,** 913–923
30. Brooks, B. R., Brooks, C. L., 3rd, Mackerell, A. D., Jr., Nilsson, L., Petrella, R. J., Roux, B., Won, Y., Archontis, G., Bartels, C., Boresch, S., Caflisch, A., Caves, L., Cui, Q., Dinner, A. R., Feig, M., *et al.* (2009) CHARMM: the biomolecular simulation program. *J. Comput. Chem.* **30,** 1545–1614
31. MacKerell, A. D., Bashford, D., Bellott, M., Dunbrack, R. L., Evanseck, J. D., Field, M. J., Fischer, S., Gao, J., Guo, H., Ha, S., Joseph-McCarthy, D., Kuchnir, L., Kuczera, K., Lau, F. T., Mattos, C., *et al.* (1998) All-atom empirical potential for molecular modeling and dynamics studies of proteins. *J. Phys. Chem. B* **102,** 3586–3616
32. Kalé, L., Skeel, R., Bhandarkar, M., Brunner, R., Gursoy, A., Krawetz, N., Phillips, J., Shinozaki, A., Varadarajan, K., and Schulten, K. (1999) NAMD2: greater scalability for parallel molecular dynamics. *J. Comp. Physics* **151,** 283–312
33. MacKerell, A. D., Jr., Feig, M., and Brooks, C. L., 3rd (2004) Improved treatment of the protein backbone in empirical force fields. *J. Am. Chem. Soc.* **126,** 698–699
34. Mackerell, A. D., Jr., Feig, M., and Brooks, C. L., 3rd (2004) Extending the treatment of backbone energetics in protein force fields: limitations of gas-phase quantum mechanics in reproducing protein conformational distributions in molecular dynamics simulations. *J. Comput. Chem.* **25,** 1400–1415
35. Darden, T., York, D., and Pedersen, L. (1993) Particle mesh ewald: an N.log(N) method for ewald sums in large systems. *J. Chem. Phys.* **98,** 10089–10092
36. Schneider, T., and Stoll, E. (1978) Molecular-dynamics study of a 3-dimensional one-component model for distortive phase-transitions. *Phys. Rev. B* **17,** 1302–1322
37. Feller, S. E., Zhang, Y. H., Pastor, R. W., and Brooks, B. R. (1995) Constant-pressure molecular-dynamics simulation: the Langevin piston method. *J. Chem. Phys.* **103,** 4613–4621